Naturally Occurring Homoisoflavonoids Function as Potent Protein Tyrosine Kinase Inhibitors by c-Src-Based High-Throughput Screening

Li-Gen Lin,[†,||] Hua Xie,[‡,||] Hong-Lin Li,[§] Lin-Jiang Tong,[‡] Chun-Ping Tang,[†] Chang-Qiang Ke,[†] Qun-Fang Liu,[†] Li-Ping Lin,[‡] Mei-Yu Geng,[‡] Hualiang Jiang,[§] Wei-Min Zhao,*[,†] Jian Ding,*[,‡] and Yang Ye*[,†]

Department of Natural Products Chemistry, Division of Anti-tumor Pharmacology and Drug Discovery and Design Center, State Key Laboratory of Drug Research, Shanghai Institute of Materia Medica, Shanghai Institutes of Biological Sciences, Chinese Academy of Sciences, 555 Zuchongzhi Road, Zhangjiang Hi-Tech Park, Shanghai 201203, People's Republic of China

Received December 3, 2007

Protein tyrosine kinase (PTK) inhibitors represent emerging therapeutics for cancer chemoprevention. In our study, hematoxylin (**26**) was identified as one of the most remarkable c-Src inhibitors in an orthogonal compound-mixing library (32200 compounds) by using an ELISA-based automated high-throughput screening (HTS) strategy. Interestingly, hematoxylin was found to be an ATP competitive broad-spectrum PTK inhibitor in vitro, with IC_{50} values ranging from nanomolar to micromolar level. Further studies showed that such inhibition was associated with the PTK phosphorylation and subsequent downstream signaling pathways. The structure−activity relationship assessment of the PTK inhibitory potency of hematoxylin analogues isolated from *Heamatoxylon campechianum* was in good agreement with the result of concurrent molecular docking simulation: the catechol moiety in ring A and the hematoxylin-like three-dimensional structure were essential for c-Src-targeted activities. Hematoxylin and its natural analogues were substantially validated to function as a new class of PTK inhibitors.

Introduction

Protein tyrosine kinases (PTKs) play crucial roles in many signal transduction pathways that regulate a variety of cellular functions, such as differentiation, proliferation, and apoptosis. Abberant activity of these kinases leads to abnormal growth control and cellular transformation, which are hallmarks of malignancy. More than 70% of the known oncogenes and proto-oncogenes involved in cancer code for PTKs. Therefore, the development of multitargeted and more effective PTKs inhibitors provides a promising opportunity for cancer therapy.[1,2] Meanwhile, with the increasing number of compounds available for screening, high-throughput screening (HTS) of chemical libraries has become a compelling approach for the discovery of novel lead compounds. Hence, it is efficient to run HTS as the initial step to develop new PTKs inhibitors as antitumor candidates.

Enzyme-linked immunosorbent assay (ELISA), a sensitive and specific assay for the detection and quantification of antigens or antibodies, has been widely used in tyrosine kinase related drug discovery research.[3,4] However, the substantial hands-on time due to washing and incubations between additions of reagents limits the efficiency of HTS performance. So it is desirable to develop a strategy for large-scale HTS with appreciable efficiency to circumvent such restriction.

In this paper, we describe an ELISA-based HTS method to identify inhibitors on c-Src (a nonreceptor tyrosine kinase)[5] kinase domain with the help of the robotic liquid handler and automated plate washer. In addition, an orthogonal compound-mixing strategy was used in the primary screening. Several novel PTKs inhibitors were identified from the library. Notably, hematoxylin (**26**) (Figure 1), a well-known natural dye isolated from the heartwood of *Haematoxylon campechianum* (Leguminosae),[6] exhibited significant PTK inhibitory activity. Moreover, we found also that hematoxylin is an ATP competitive broad-spectrum inhibitor of PTK both at enzymatic and cellular level. The stems of *H. campechianum* were chemically investigated using the bioassay-guided approach for the purpose of finding out its novel bioactive analogues. Ten novel homoisoflavonoids (**1**−**10**) and 16 known ones (**11**−**26**) (Figure 1) were identified. Moreover, the structure−activity relationship of these compounds was established by chemical analysis and computer molecular docking simulation. The results show that the catechol moiety in ring A and the hematoxylin-like three-dimensional structure were essential for the inhibitory activity on PTKs. Hematoxylin and a series of its natural analogues were first reported as a new class of potent PTK inhibitors.

Results

High-Throughput Screening of c-Src Tyrosine Kinase Inhibitors. The optimized c-Src-based ELISA assay was used to high-throughput screen 32200 single compounds, which represent a wide variety of chemical structures. Orthogonal compound-mixing strategy as well as robotic liquid handler and automated microtiter plate washer were used in the primary screening, which resulted in high assay speed and better performance. After the primary screen compounds tested at a single concentration of 0.01 mg/mL, all primary hits demonstrating at least 30% inhibition relative to control were retested to confirm activity, and finally, 31 potential inhibitors were confirmed (data not shown). Notably, one known compound hematoxylin, a widely used nuclei dye, was revealed to be one of the most potent inhibitors of c-Src tyrosine kinase, with IC_{50} value at 440 nM (Table 1). Therefore, our subsequent work mainly focused on the PTK inhibitory effects of this compound and its newly isolated analogues.

* To whom all correspondence should be addressed. For Y.Y.: Phone, +86 21 50806600 ext 3326; Fax, +86 21 50806726; E-mail, yye@mail.shcnc.ac.cn. For J.D.: Phone, +86 21 50806600 ext 2423; Fax, +86 21 50806722; E-mail, jding@mail.shcnc.ac.cn. For W.-M.Z.: Phone/Fax, +86 21 50806052; E-mail, wmzhao@mail.shcnc.ac.cn.

† Department of Natural Products Chemistry.

|| Those authors contributed equally.

‡ Division of Antitumor Pharmacology.

§ Drug Discovery and Design Center.

10.1021/jm701501x CCC: $40.75
Published on Web 07/09/2008

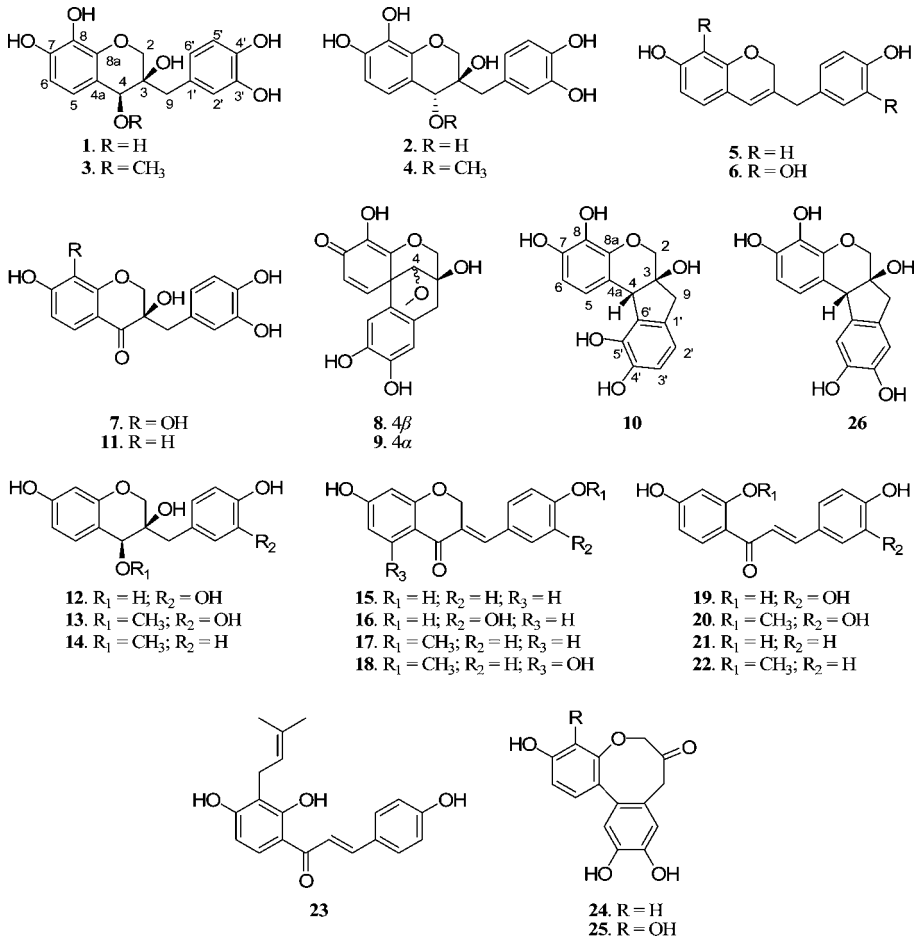

Figure 1. Chemical structures of homoisoflavonoids and chalcones (**1**−**26**) from *H. campechianum*.

Table 1. Effects of Hematoxylin (**26**) on Tyrosine Kinases Activities in Cell-Free System[a]

kinase	IC_{50} (μM)	maximum inhibition rate (%) at 10 μM [b]
c-Src	0.44 ± 0.12	95.1
c-Met	0.40 ± 0.08	100.0
FGFR1	0.32 ± 0.13	98.2
ErbB2	0.96 ± 0.25	97.6
KDR	2.10 ± 0.49	81.8
Flt-1	2.90 ± 0.30	79.6
EGFR	3.40 ± 0.63	73.2
PDGFR	5.00 ± 1.82	93.6
c-Kit	2.70 ± 0.99	86.2
EphB2	>10	44.3

[a] The inhibition rate (%) was calculated using the equation: [1 − (A_{490}/A_{490} control)] × 100%. IC_{50} values were determined from three separate experiments; each compound concentration was tested in duplicate. [b] Values are means of three determinations and deviation from the means is <10% of the mean value.

Hematoxylin Broadly Inhibits Tyrosine Kinase Activity. We next examined whether hematoxylin inhibited the kinase activities of other related tyrosine kinases at enzymatic level. As shown in Table 1, hematoxylin not only exhibited potent inhibitory activity on c-Src but also produced remarkable inhibitory effects on c-Met, FGFR1, and ErbB2, with IC_{50} values at nanomolar level. In addition, it also exhibited powerful inhibitory effects on KDR, Flt-1, c-Kit, EGFR, and PDGFRβ, with IC_{50} values at low micromolar level. Meanwhile, we noted that it possessed weak inhibitory effect on EphB2 with IC_{50} value more than 10 μM. These results revealed that hematoxylin is an effective broad-spectrum inhibitor of PTK.

Hematoxylin is a Competitive Inhibitor with ATP on c-Src. Most of the small molecule inhibitors of PTK are ATP competitive by binding to the ATP-pocket of the kinase domain. Therefore, further research was performed to identify whether hematoxylin is an ATP-competitive inhibitor of c-Src. Kinase assays were performed as describe in Experimental Section by ELISA method with various concentrations of ATP. The values from individual samples were analyzed and plotted as a function of drug concentration (Figure 2A) and were fitted to the Sigmoidal dose−response equation (Figure 2B) by using Graphpad Prism 4.0 software. The results clearly indicated that with the increasing concentration of ATP, the IC_{50} values were increased correspondingly, supporting that hematoxylin is a competitive inhibitor with ATP on c-Src tyrosine kinase.

Hematoxylin Blocks Tyrosine Kinase Phosphorylation and Arrests Downstream Signaling Pathways in Cellular Level. We further determined the ability of hematoxylin to inhibit the PTKs in intact cells. HT-29 cell (high c-Src expression and activity) and SK-OV-3 cell (which is known to overexpress ErbB2) were selected for detecting the expression of c-Src and ErbB2, respectively. Western blotting results showed that hematoxylin inhibited the autophosphorylation of c-Src and paxillin,[7] a substrate of c-Src (Figure 3A), as well as the EGF-induced-phosphorylation of ErbB2 (Figure 3B) in a dose-dependent manner. The overall levels of them were not affected in treated cells.

Phosphorylation of receptor tyrosine kinases leads to activation of a number of downstream cytoplasmic signaling cascades that are central to tumor growth and angiogenesis. We thus further studied the effects of hematoxylin on the downstream

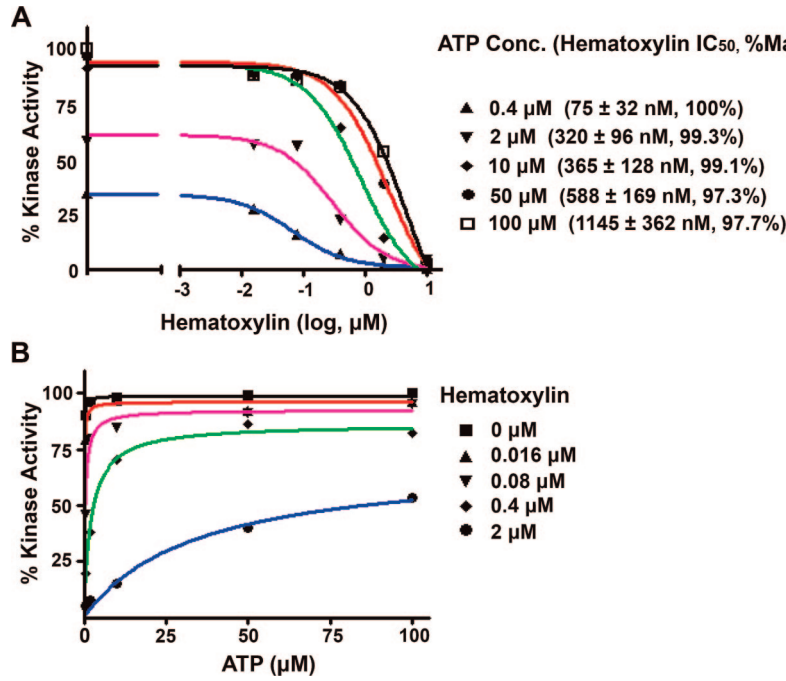

Figure 2. Steady-state kinetic analysis of c-Src kinase inhibition by hematoxylin. (A) C-Src kinase inhibition assays were performed by ELISA assay as described in the Experimental Section in a reaction mixture containing various concentrations of ATP. The level of kinase activity is expressed as a percent of the maximal kinase activity. For calculating IC_{50} values, the inhibition rate (%) was calculated using the equation $[1 - (A_{490}/A_{490}\ \text{control})] \times 100\%$. IC_{50} values were obtained by Logit method and were determined from the results of at least three independent tests. (B) The curves represent calculated best fits to the sigmoidal dose−response equation with various amounts of ATP and hematoxylin. % max: maximum inhibition rate at 10 μM.

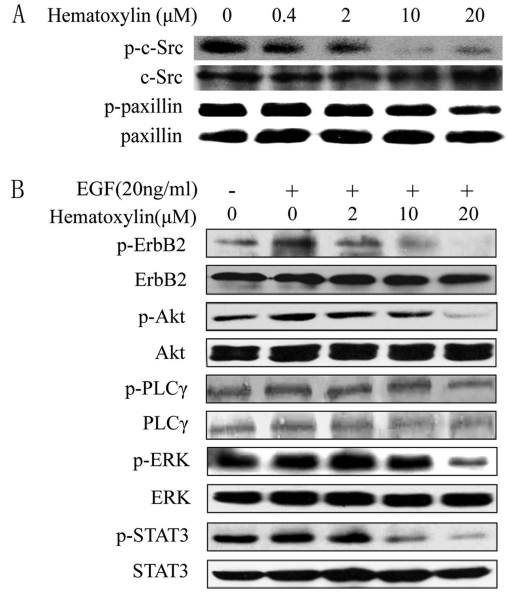

Figure 3. Effects of hematoxylin on the phosphorylation of c-Src and paxillin in HT-29 cells (A) and on the phosphorylation of ErbB2 and downstream signaling in SK-OV-3 cells (B). Data shown are representative of three independent Western blotting assays.

signaling cascades of ErbB2 receptors in SK-OV-3 cells. Results revealed that hematoxylin inhibited EGF-induced activation of ERK1/2, AKT, and STAT3 in a dose-dependent manner but showed weak effect on PLCγ. The total protein levels of them were similar in the presence and absence of hematoxylin (Figure 3B).

These results showed that hematoxylin can block the phosphorylation of PTK in cellular level and therefore arrest the downstream signaling pathways.

Isolation and Structural Elucidation of Homoisoflavonoids. To find novel hemotoxylin analogues with potent inhibitory activities on PTKs, the stems of a homoisoflavonoid-rich plant, *H. campechianum*, were investigated extensively. Bioassay-directed fractionation of the dichloromethane fraction (30 g) and ethyl acetate fraction (110 g) of the extract of this plant by repeated flash column chromatography, as detailed in the Experimental Section, led to the isolation of 10 new homoisoflavonoids, namely hematoxylol (**1**), epihematoxylol (**2**), 4-*O*-methylhematoxylol (**3**), 4-*O*-methylepihematoxylol (**4**), sappanene (**5**), hematoxylene (**6**), hematoxylone (**7**), hematoxin (**8**), epihematoxin (**9**), and isohematoxylin (**10**), as well as 16 known compounds (**11**−**26**) (Figure 1). The known compound hematoxylin (**26**) was identified by direct comparison with the authentic sample (co-TLC, ^{1}H NMR, MS). The structures of sappanone B (**11**),[8] sappanol (**12**),[9] 4-*O*-methylsappanol (**13**),[8] 3′-deoxy-*O*-methylsappanol (**14**),[8] 3′-deoxy-sappanone A (**15**),[10] sappanone A (**16**),[8] bonducellin (**17**),[11] (*E*)-eucomin (**18**),[12] butein (**19**),[9] sappanchalcone (**20**),[8] isoliquiritigenin (**21**),[8] 3′-deoxy-sappanchalcone (**22**),[8] isobavachalcone (**23**),[13] protosappanin A (**24**),[14] and hematoxylol (**25**)[15] were identified by comparison of their spectroscopic data (^{1}H, ^{13}C NMR, MS) with those reported. The structures of the new compounds **1**−**10** have been deduced as followed.

Haematoxylol (**1**) was obtained as a yellow amorphous powder. The molecular formula was established as $C_{16}H_{16}O_7$ by HRESIMS, with nine degrees of unsaturation. The IR absorptions at 3415 and 1624 cm^{-1} indicated the presence of hydroxyl groups and benzenoid moieties. The ^{13}C NMR and DEPT spectra indicated 16 carbon signals, ascribed to two benzene rings, two oxymethines, and two methylenes (Table 2). The ^{1}H NMR spectrum displayed the resonances of an aromatic ABX system [δ 6.62 (d, J = 8.0 Hz), 6.51 (dd, J = 1.8, 8.0 Hz), 6.63 (d, J = 1.8 Hz)], two geminal protons at δ

Table 2. ^{13}C NMR Data of Homoisoflavonoids **1**−**10** (**1**−**9** in CD_3OD, **10** in CD_3COCD_3, 100 MHz)

position	1	2	3	4	5	6	7	8	9	10
C-2	68.7	68.7	68.7	79.8	68.5	69.4	72.9	76.2	79.8	70.3
C-3	71.6	71.5	71.6	71.9	131.4	133.0	73.3	70.4	71.9	79.2
C-4	80.4	70.7	80.5	86.8	120.2	121.5	194.5	86.6	86.8	51.1
C-4a	114.4	117.5	114.3	96.5	115.9	117.8	113.1	55.0	54.0	118.4
C-5	123.0	122.2	123.0	114.2	127.7	118.1	119.1	150.3	149.2	120.9
C-6	109.4	110.3	109.4	149.3	108.9	109.5	111.0	130.6	129.8	109.7
C-7	148.0	147.3	148.1	150.5	158.8	147.5	152.6	186.2	185.3	144.2
C-8	134.8	134.3	134.8	136.5	103.3	134.4	133.1	136.8	136.2	133.1
C-8a	143.9	144.1	143.9	153.8	155.0	142.7	151.0	153.3	153.8	142.3
C-9	41.4	41.6	41.4	39.4	39.3	40.5	40.3	43.9	39.5	41.5
C-1′	129.4	129.6	129.4	128.9	129.6	131.5	127.3	127.9	129.0	134.3
C-2′	119.6	119.5	119.6	115.8	130.7	117.4	118.4	116.6	116.8	116.2
C-3′	146.1	146.2	146.1	146.7	116.1	146.8	145.0	147.2	146.7	114.6
C-4′	145.4	145.4	145.4	145.4	156.9	145.4	144.4	145.7	145.5	144.0
C-5′	116.2	116.4	116.2	116.7	116.1	116.8	115.2	114.0	114.2	143.1
C-6′	123.8	123.7	123.8	125.1	130.7	121.8	122.7	126.3	125.1	132.4
OMe-4			57.5	62.9				62.8	62.9	

Table 3. ^1H NMR Data of Homoisoflavonoids **1**−**5** (in CD_3OD, 400 MHz, *J* in Hz)

no.	1	2	3	4	5
H-2α	3.93d (10.2)	3.97d (10.2)	3.98d (9.8)	4.17d (11.5)	
H-2*β*	3.77d (10.2)	3.77d (10.2)	3.78dd (1.2,9.9)	3.91dd (1.2,11.5)	4.56s (2H)
H-4	4.23s	3.70s	3.70d (1.1)	3.60d (1.2)	6.10 bs
H-5	6.53d (8.2)	6.64d (8.2)	6.55d (8.4)	6.37d (8.3)	6.88d (8.1)
H-6	6.42d (8.2)	6.43d (8.2)	6.45d (8.4)	6.52d (8.2)	6.32dd (2.3,8.1)
H-8					6.24d (2.3)
H-9	2.62s (2H)	2.84d (13.8)2.70d (13.9)	2.56s (2H)	2.83d (13.5)2.65d (13.5)	3.35s (2H)
H-2′	6.63d (1.8)	6.68d (1.8)	6.64d (0.9)	6.79d (1.7)	7.07d (6.3)
H-3′					6.87d (6.3)
H-5′	6.62d (8.0)	6.64d (8.0)	6.63d (8.0)	6.70d (8.3)	6.87d (6.3)
H-6′	6.51dd (1.8,8.0)	6.43dd (1.8,8.0)	6.44dd (0.9,8.0)	6.61dd (1.7,8.3)	7.07d (6.3)
OMe			3.32s	3.32s	

3.93 (d, $J = 10.2$ Hz) and 3.77 (d, $J = 10.2$ Hz), one oxygenated proton at δ 4.23 (s), and two protons at δ 2.62 (s) (Table 3). These resonances were indicative of a sappanol-type homoisoflavonoid.[8–12] In comparison with sappanol (**12**), two *ortho*-position aromatic protons [δ 6.53 (d, $J = 8.2$ Hz), 6.42 (d, $J = 8.2$ Hz)] instead of another ABX system were observed in the molecule of **1**. The doublet proton (δ 6.53) was assigned at C-5 by the correlations from this proton to C-4, C-7, and C-8a in the HMBC spectrum (as shown in Figure 4). Furthermore the proton at δ 6.42 was designated as H-6, and positions 7 and 8 were substituted by two hydroxyl groups. Such a structural moiety was confirmed by the HMBC correlation between H-6 and C-8. Therefore, compound **1** was determined as an 8-hydroxyl derivative of sappanol. The relative configuration of **1** was established as the same as that of sappanol. The $3R^*$-configuration was determined based on the biogenetic relationship. The hydroxyl group at C-4 was β-oriented by the ROESY cross-peak between H-4 and H-2α, and this $4S^*$-configuration was further supported by the chemical shifts and splitting mode of H-9 (δ 2.62, s).[16] Accordingly, compound **1** was elucidated to be ($3R^*$,$4S^*$)-3-(3,4-dihydroxylbenzyl)-3,4,7,8-tetrahydroxylchroman. The ^1H and ^{13}C NMR spectroscopic data were completely assigned (Tables 2 and 3) by extensive analyses of the 1D and 2D NMR (^1H, ^{13}C NMR, ROESY, HSQC, and HMBC) spectra.

Epihematoxylol (**2**) was obtained as a brown amorphous powder. Its molecular formula was determined as $C_{16}H_{16}O_7$ by HRESIMS at *m*/*z* 343.0782 $[M + Na]^+$ (calcd 343.0794). The IR absorptions at 3410 and 1624 cm^{-1} indicated the existence of hydroxyl groups and benzenoid moieties. A careful analysis of its ^1H and ^{13}C NMR data (Tables 2 and 3) revealed that **2** was a stereo isomer of **1**. In the ^1H NMR spectrum of **2** the methylene protons at C-9 resonated as two doublets [δ 2.84 (d, $J = 13.8$ Hz), 2.70 (d, $J = 13.9$ Hz)], suggesting that the hydroxyl group at C-4 was α-oriented.[13] The ROESY correlation between H-4 and H-2*β* confirmed the above conclusion. Thus compound **2** was determined to be ($3R^*$,$4R^*$)-3-(3,4-dihydroxylbenzyl)-3,4,7,8-tetrahydroxylchroman.

4-*O*-methylhematoxylol (**3**) and 4-*O*-methylepihematoxylol (**4**) were obtained as brown amorphous powders. Their molecular formulas were deduced as $C_{17}H_{18}O_7$ by HRESIMS spectra

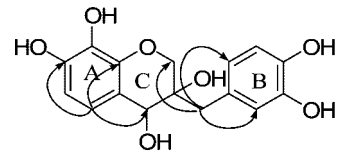

1

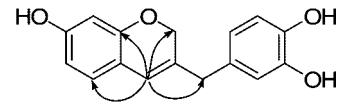

5

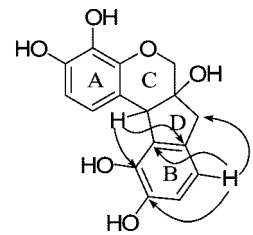

10

Figure 4. Key HMBC correlations of compounds **1**, **5**, and **10** (H → C).

Table 4. ^{1}H NMR Data of Homoisoflavonoids **6**−**10** (**6**−**9** in CD_3OD, **10** in CD_3COCD_3, 400 MHz, *J* in Hz)

no.	6	7	8	9	10
H-2α	4.55s (2H)	4.21d (10.9)	4.07d (10.7)	4.14d (10.4)	4.18d (10.6)
H-2β		4.02d (10.8)	4.02d (10.7)	3.71dd (2.1,10.7)	3.83d (10.5)
H-4	6.10s		3.82s	3.38s	4.34s
H-5	6.33d (8.3)	7.30d (8.7)	7.01d (9.6)	7.14d (10.0)	7.31d (8.3)
H-6	6.29d (8.3)	6.63d (8.9)	6.50d (9.7)	6.54d (10.0)	6.39d (8.3)
H-9	3.26s (2H)	2.85d (14.0)	3.17d (3.4, 2H)	3.30d (6.1)	3.22dd (1.3,15.7)
		2.77d (13.9)		2.90d (6.1)	2.69d (15.8)
H-2′	6.66d (2.4)	6.80d (1.9)	6.58s	6.58s	6.48d (7.8)
H-3′					6.61d (7.8)
H-5′	6.69d (7.9)	7.30d (8.1)	6.31s	6.30s	
H-6′	6.54dd (2.4,7.9)	6.60dd (2.0,8.0)			
OMe			3.52s	3.59s	

[**3**: *m/z* 357.0945 $[M + Na]^+$; **4**: *m/z* 357.0918 $[M + Na]^+$ (calcd 357.0950)]. Both IR spectra suggested the presence of hydroxyl groups and benzenoid moietes. A careful analysis of their NMR data revealed that these two compounds were a pair of stereoisomers. The ^{1}H and ^{13}C NMR spectra of **3** (Tables 2 and 3) strongly resembled those of **1**, except for an additional methoxyl resonance. The methoxyl group was assigned at C-4 by the HMBC correlations between the methoxyl (δ 3.32) and C-4 and between H-4 and the methoxyl carbon (δ 57.5). Therefore compound **3** was determined as (3*R**,4*S**)-3-(3,4-dihydroxylbenzyl)-3,7,8-trihydroxyl-4-methoxylchroman. Such a structure was further confirmed by ROESY and HMBC experiments. Similarly, compound **4** was elucidated as the 4-methoxyl derivative of compound **2** and designated as (3*R**,4*R**)-3-(3,4-dihydroxylbenzyl)-3,7,8-trihydroxyl-4-methoxylchroman.

Sappanene (**5**) was obtained as a yellow amorphous powder. Its molecular formula, $C_{16}H_{14}O_3$, was inferred by its quasimolecular ion at *m/z* 254.0940 $[M]^+$ (calcd 254.0943) in HREIMS. The presence of hydroxyl groups and benzenoid moieties could be judged from the absorption bands at 3423 and 1618 cm^{-1} in the IR spectrum. The ^{1}H NMR spectrum displayed resonances of one 1,2,4-trisubstituted benzene ring and one *para*-disubstituted benzene ring (Table 3). These structural moieties were the same as rings A and B of 3′-deoxy-sappanone.[8] Three singlet resonances were also observed at δ 6.10 (br s, 1H), 4.56 (s, 2H), and 3.35 (s, 2H) in the ^{1}H NMR spectrum. The singlet olefinic proton at δ 6.10 was assigned as H-4 by the HMBC correlations from this proton to C-5 and C-8a. The singlet methylene at δ 3.35 was inferred as H-9 by the HMBC correlations from it to C-4 and C-2′ (6′). The other methylene was assigned as H-2, which was supported by the HMBC cross-peaks from the methylene to C-4, C-8a, and C-9 (Figure 4). These evidence suggested a 3,4-ene ring C. Thus the structure of **5** was elucidated to be 3-(4-hydroxylbenzyl)-7-hydroxyl-chroman-3,4-ene.

Haematoxylene (**6**), a brown amorphous powder, showed the molecular formula as $C_{16}H_{14}O_5$ by HRESIMS at *m/z* 309.0767

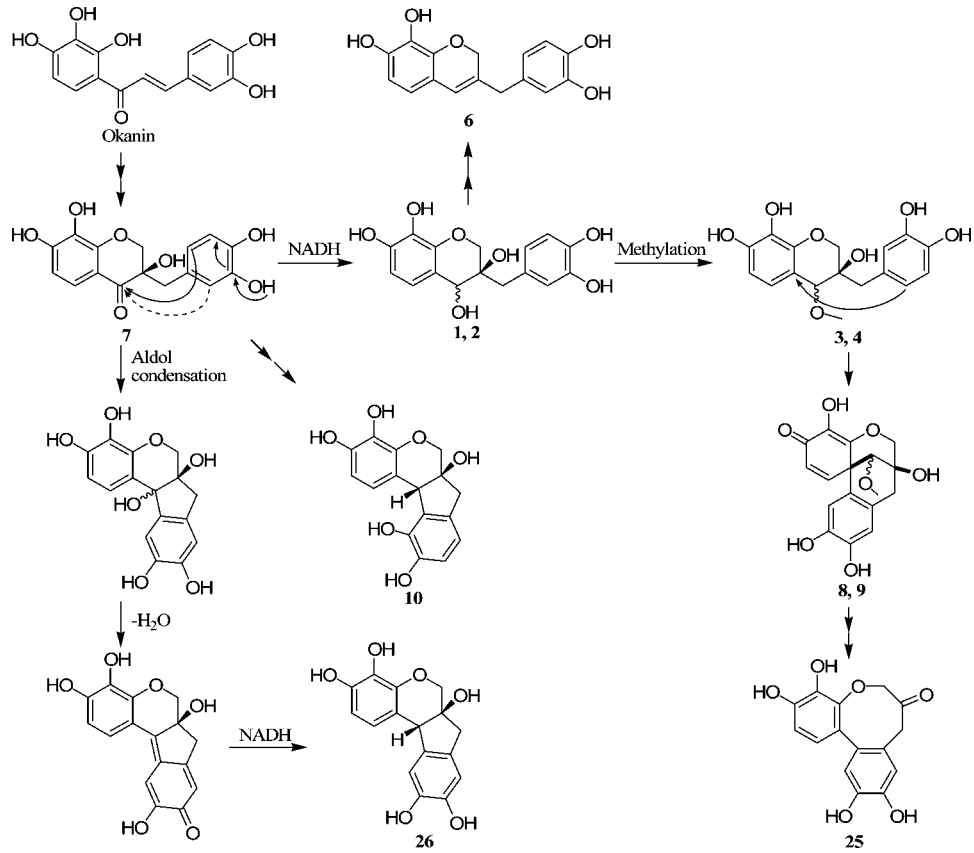

Figure 5. Proposed biogenetic pathway for homoisoflavonoids.

Table 5. Inhibitory Rates of All Isolates on Several PTKs Assay (10 μM) by Using ELISA Method[a]

	inhibitory rates (%)						
compound	c-Src	KDR	c-kit	EGFR	FGFR1	FGFR2	c-Met
1	64.1	89.9	81.6	62.8	99.4	75.5	88.6
2	91.0	95.3	93.2	66.6	97.5	84.9	96.2
3	25.7	86.2	66.1	54.5	93.3	60.3	79.5
4	74.4	64.0	ND	ND	ND	ND	84.6
5	0	9.1	6.7	2.9	14.4	0	ND
6	87.5	86.8	79.2	52.7	99.4	62.6	91.3
7	94.8	84.8	89.6	86.2	96.7	91.5	93
8	0	9.9	9.4	3.6	27.9	3.1	ND
9	0.3	25.0	16.3	14.5	48.1	35.2	86.1
10	87.1	81.2	68.6	42.3	94.3	35.2	87.2
11	82.1	54.2	ND	ND	ND	ND	ND
12	77.4	51.1	ND	ND	ND	ND	ND
13	0	7.2	5.2	5.2	24.2	8.8	ND
14	0	3.1	19.8	2.8	13.8	0	ND
15	1.6	59.2	35.4	0	76.2	0	37.4
16	7.7	52.0	17.5	6.4	69.5	17.7	56.6
17	0	13.8	6.0	0	6.7	0	ND
18	0.7	1.2	2.3	0	0	0	ND
19	9.1	48.3	15.1	3.0	68.5	3.0	81.7
20	33.3	83.5	44.7	26.7	86.9	48.5	64.3
21	0	14.0	10.8	0	13.1	0	ND
22	1.0	12.3	1.7	0	28.0	0	ND
23	50.1	58.4	ND	ND	ND	ND	ND
24	0	3.6	0	0.9	29.0	0	ND
25	94.4	93.0	90.4	83.2	98.4	54.8	87.4
26	95.4	99.5	97.2	92.4	100.0	73.6	100.0

[a] The inhibitory rates (%) were determined from the results of three separate tests ($n = 3$) and calculated using the equation: $[1 - (A_{490}/A_{490}$ control$)] \times 100\%$. ND: not determined.

$[M + Na]^+$ (calcd 309.0739). The IR absorption bands at 3424 and 1623 cm^{-1} indicated the existence of hydroxyl groups and benzenoid moieties. The ^1H NMR spectrum displayed resonances of an aromatic ABX system and two *ortho*-position aromatic protons, which resembled the corresponding signals of rings A and B of compound **1**. The remaining resonances constructed the same ring C as that of **5** by comparison of their ^1H and ^{13}C NMR data. The structure was confirmed by HSQC and HMBC experiments. Thus **6** was determined to be 3-(3,4-dihydroxylbenzyl)-7,8-dihydroxylchroman-3,4-ene.

Haematoxylone (**7**) was obtained as a yellow amorphous powder. The molecular formula was inferred as $C_{16}H_{14}O_7$ by HRESIMS at *m/z* 341.0655 $[M + Na]^+$ (calcd 341.0637). The presence of hydroxyl groups and benzonoid moieties were indicated by IR absorption bands at 3325 and 1637 cm^{-1}. In the ^1H NMR spectrum, the aromatic signals were similar to those of **1** (Table 4), indicating that **7** shared the same substituted pattern of rings A and B as those of **1**. Additionally two sets of germinal doublet signals [δ 4.21 (d, $J = 10.9$ Hz) and 4.02 (d, $J = 10.8$ Hz); 2.85 (d, $J = 14.0$ Hz) and 2.77 (d, $J = 13.9$ Hz)] were observed. The ^{13}C NMR spectrum, besides those aromatic carbons, exhibited a carbonyl carbon (δ 194.5), two methylene carbons (δ 72.9 and 40.3), and a quaternary carbon (δ 73.3) (Table 2). These evidence suggested a 3-ol-4-one moiety in ring C of **7**, the same as that of sappanone B (**11**).[8] Therefore, the structure of **7** was determined to be (3*R**)-3-(3,4-dihydroxybenzyl)-3,7,8-trihydroxychroman-4-one.

Haematoxin (**8**) and epihematoxin (**9**) were obtained as brown amorphous powders. Their molecular formulas, $C_{17}H_{16}O_7$, were inferred from HRESIMS spectra [**8**: *m/z* 355.0797 $[M + Na]^+$; **9**: *m/z* 3555.0800 $[M + Na]^+$ (calcd 355.0794)]. The IR spectra showed absorptions due to an α,β-unsaturated ketone (**8**: 1641; **9**: 1643 cm^{-1}), an aromatic ring (**8**: 1593; **9**: 1595 cm^{-1}), and a hydroxyl group (**8**: 3385; **9**: 3404 cm^{-1}). The ^1H and ^{13}C NMR spectra of **8** and **9** resembled each other strongly (Tables 2 and 4), and both displayed the resonances of a methoxyl, an oxymethylene, an oxymethene, an $\alpha,\alpha',\beta,\beta'$-unsaturated ketone system, and a tetra-substituted benzene ring. These spectroscopic data were very similar to those of caesalpin J.[17] The major difference observed was that two *ortho*-position protons in **8** and **9** replaced the ABX system protons in caesalpin J, which indicated that a hydroxyl group was attached to C-8. Therefore, compounds **8** and **9** were determined as 8-hydroxyl derivatives of caesalpin J. Their structures were confirmed by HSQC and HMBC experiments. The configurations of these two compounds were revealed by ROESY spectra. The hydroxyl group at C-3 was in β-orientation on biogenetic consideration. The methoxyl group at C-4 in **8** was assigned as β-oriented by the NOE correlations between H-4 and H-9 and OMe-4 and H-2β, while that in **9** was α-oriented by the NOE cross peaks between H-4 and H-2β and OMe-4 and H-9. Accordingly, compounds **8** and **9** were determined to be a pair of C-4 stereoisomers.

Isohematoxylin (**10**) was obtained as a yellow amorphous powder. The ion peak at *m/z* 325.0673 $[M + Na]^+$ in the HRESIMS established the molecular formula as $C_{16}H_{14}O_6$. The presence of hydroxyl groups and benzenoid moieties could be judged from the absorption bands at 3406 and 1618 cm^{-1} in the IR spectrum. Most of its NMR data (Tables 2 and 4) resembled those of hematoxylin (**26**), except resonances of two *ortho*-position aromatic protons [δ 6.61 (d, $J = 7.8$, 1H) and 6.48 (d, $J = 7.8$, 1H)], which were observed as two singlet signals in the ^1H NMR spectrum of hematoxylin. These two *ortho*-coupled protons were assigned as H-2′ and H-3′, and such substituent was supported by the HMBC cross-peaks from H-2′ to C-9, C-4′ and C-6′, and from H-4 to C-1′ and C-5′ (as shown in Figure 4). Compound **10** was believed to be a byproduct in biogenetic synthesis of hematoxylin, and was nominated as isohematoxylin.

Proposed Biogenetic Pathway of Homoisoflavonoids. A plausible biogenetic pathway for homoisoflavonoids is proposed as shown in Figure 5. All homoisoflavonoid compounds can be considered as precursors or byproduct of hematoxylin. Hemoatoxylone (**7**) appears to be the first homoisoflavonoid generated from a chalcone okanin.[18] Subsequently, through an aldol condensation of C-6′ and C-4 carbonyl group, dehydration, and then reduction, compound **7** was transformed to the end product hematoxylin (**26**). In this course, many homoisofla-

Table 6. Inhibitory Activities of Four Active Compounds against Five Selected Kinases by using ELISA Assay[a]

	c-Src		c-Met		FGFR1		c-Kit		KDR	
compd	$IC_{50}(\mu M)$	% max [b]	$IC_{50}(\mu M)$	% max [b]	$IC_{50}(\mu M)$	% max [b]	$IC_{50}(\mu M)$	% max [b]	$IC_{50}(\mu M)$	% max [b]
2	0.36 ± 0.03	90.8	0.36 ± 0.16	95.3	0.56 ± 0.02	86.6	0.70 ± 0.05	94.6	2.10 ± 1.27	87.7
6	1.60 ± 0.75	83.0	0.76 ± 0.14	92.0	0.60 ± 0.25	77.8	5.90 ± 0.49	84.0	8.60 ± 3.07	64.4
7	1.80 ± 0.21	86.7	0.85 ± 0.14	93.5	2.90 ± 0.08	81.7	3.20 ± 0.74	90.3	6.10 ± 3.63	75.7
26	0.44 ± 0.12	95.1	0.40 ± 0.08	100	0.32 ± 0.13	98.2	2.70 ± 0.99	86.2	2.10 ± 0.49	81.8

[a] The inhibition rate (%) was calculated using the equation: $[1 - (A_{490}/A_{490}$ control$)] \times 100\%$. IC_{50} values were obtained by Logit method based on the data obtained from three separate experiments; each compound concentration was tested in duplicate. % max: maximum inhibition rate at 10μM. [b] Values are means of three determinations and deviation from the means is <10% of the mean value.

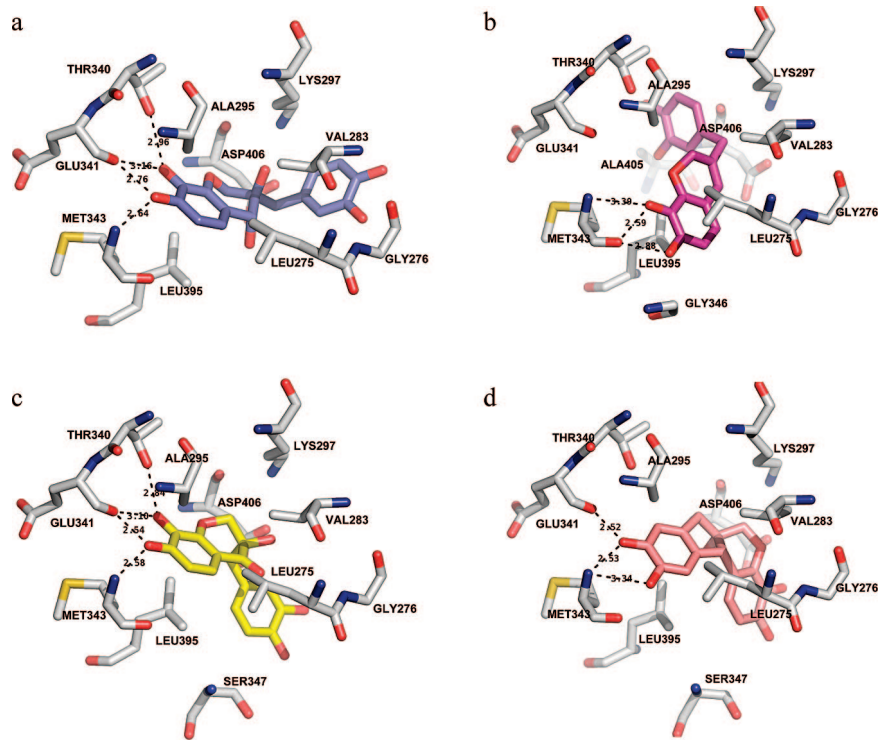

Figure 6. The binding modes of compounds **2** (a), **6** (b), **7** (c), and **26** (d) to the kinase domain of c-Src predicted by the molecular docking simulations. The inhibitions and residues (gray) are represented as stick. The black dashed lines denote the hydrogen bonds. The carbon atoms for each compound are colored as follows: (a) compound **2**, purple; (b) compound **6**, magenta; (c) compound **7**, yellow; (d) compound **26**, salmon. The coloring for oxygen atoms of each compound is red. All structure figures were prepared using PyMol (http://pymol.sourceforge.net/).

vonoids could be obtained as the byproduct. The C-4 carbonyl group in compound **7** would be reduced to a hydroxyl group nonselectively to produce compounds **1** and **2**, which could be methylated to form **3** and **4**, respectively. Cyclization between C-4a and C-6′ by a nucleophilic addition in **3** and **4** would result in compounds **8** and **9**, respectively. Further oxidation of **8** and **9** yielded finally compound **25**. In another way, the non-predominant compound **10** could also be produced if compound **7** was subjected to an aldol condensation of C-2′ and the carbonyl group. Additionally, the vicinal diol in **1** and **2** could be reduced to give compound **6**.

Inhibitory Activities Evaluation on PTKs Assay of all Isolates. All the isolates, including hematoxylin, were assayed for the inhibitory activities on seven PTKs (KDR, c-kit, c-Src, c-Met, EGFR, FGFR1, and FGFR2) in vitro. As shown in Table 5, compounds **1**, **2**, **3**, **4**, **6**, **7**, **10**, **11**, **20**, **25**, and **26** possessed effective inhibitory activities on most of the PTKs tested, yielding inhibitory rate more than 80% at 10 μM concentration. Meanwhile, compounds **12**, **15**, **16**, **19**, and **23** showed slightly weaker inhibitory effects than compound **26**, with inhibitory rate >50% at 10 μM concentration. Other analogues, however, failed to inhibit the PTKs tested.

Furthermore, four active compounds, **2**, **6**, **7**, and **26**, were tested IC_{50} values on five selected PTKs (Table 6). As expected, these compounds produced remarkable inhibitory effects on the tyrosine kinases with IC_{50} values ranging from nanomolar to low micromolar level, particularly effective on c-Met with nanomolar potency. In addition, we noted that compounds **2** and **26** possessed much more effective inhibitory activities than compounds **6** and **7**. Notably, compound **2** exhibited much powerful effect on c-Kit than other compounds tested, with IC_{50} value at 0.70 μM.

Docking Analysis of Hematoxylin with c-Src Tyrosine Kinase Domain. To explore the binding characteristics of the compounds, the binding models of four representative compounds (**2**, **6**, **7**, and **26**) with c-Src tyrosine kinase domain were constructed based on molecular docking simulation (see Experimental Section). Figure 6 shows the interaction models of four potent inhibitors to c-Src, indicating that these inhibitors occupy the adenine pocket of the ATP binding site instead of the triphosphate pocket. The binding orientation of all the compounds is almost the same, which locates at the hinge region through H-bonds with amino acid residues. The binding models (Figure 6a−d) indicate that compounds **2** and **7** interact with the hinge region in the same way, there are four H-bonds between catechol fragment of compounds **2** and **7** and the hinge region: one to the amide nitrogen of Met343, two to the carbonyl of Glu341, and another one to the side-chain of Thr340. There are also extensive hydrophobic interaction and van der Waals contacts to the hinge region residues (Met343, Glu341 and Thr340). The second catechol fragment stretched deeply into a binding pocket with hydrophobic interaction, which was surrounded by residues from β-sheet 3 (Ala295 and Lys297), the glycine loop (Leu275 and Val283), β-strand 7 (Leu395), and the conserved DFG-motif of the activation loop (Asp406). However, compound **26** binds to the pocket with three H-bonds at the hinge region (the amide nitrogen of Met343 and carbonyl of Glu341), similarly, other hydrophobic and van der Waals contacts interactions are the same compared with the above two compounds (Figure 6d). There are three H-bonds from the catechol groups of compound **6** to the carbonyl and amide of Met343, and the second catechol fragment presented different orientation compared with above-mentioned three compounds (compounds **2**, **7**, and **26**). The autodock results indicated that the representative compounds have good interaction with the

enzyme active site, moreover, they may exert their tyrosine kinase inhibitory activity in an ATP-competitive manner.

Discussion

Some small molecule PTK inhibitors, such as imatinib and dasatinib, have already shown the unique efficacy in chemotherapy, and many more candidates are in clinical or preclinical studies.[19,20] However, several promising candidates failed in clinical trials due to the complex nature of signal crosstalking. It is increasingly recognized that PTK inhibitors with broad-spectrum, which multitarget malignant cells, would achieve a better clinical benefit than selective ones.[21] Two recently approved multitargeted PTK inhibitors by FDA/EMEA, sorafenib and sunitinib, marked a new generation of PTK inhibiting agents.[22,23] So it is expected that the development of effective multitargeted PTK inhibitors would provide a promising therapeutic opportunity against cancer.

C-Src, a nonreceptor tyrosine kinase, exhibits elevated protein level activity in numerous types of human cancers and functions as a critical component in the multiple signaling pathways that regulate proliferation, survival, metastasis, and angiogenesis.[5] We have successfully expressed large amount of c-Src (kinase domain) with high kinase activity using Bac-to-Bac baculovirus expression system in our laboratory. Therefore, in the present work, c-Src was preferentially selected for the establishment of the high-throughput platform for primary screening of PTK inhibitors, which was followed by the comprehensive evaluation of the PTK inhibitory activities of the hits for the purpose of seeking broad-spectrum PTK inhibitors.

Several PTK assays have been used to test protein kinase activity, including ELISA, $^{32}PO_4$-transfer assay, DELFIA (fluorometric), HTRF (homogeneous time-resolved fluorescence), SPA (scintillation proximity assay), and fluorescence depolarization (FP) assay. Though ELISA is noted for its intensive labor due to the plate-coating and several washing steps, this approach is specific, sensitive, and in particular, free of radiolabeling and less costly. Therefore, the ELISA-based HTS platform with the intended introduction of the orthogonal compound-mixing strategy, the robotic liquid handler, and automated plate washer was preferentially developed to overcome this intrinsic limitation in the present study. All these techniques provide this newly improved ELISA assay as a simple and convenient method suitable for HTS of PTK inhibitors.

With the availability of this platform, 32200 compounds were screened, and 31 compounds were identified to inhibit c-Src activity in the nanomolar to micromolar range. Hematoxylin, a well-known dye,[24] was found to be a potent inhibitor of c-Src and a broad-spectrum PTK inhibitor both at enzymatic and cellular level as well. Moreover, hematoxylin inhibited several major growth factor-induced signaling effectors associated with the Ras-Raf-MAPK, PI3K-AKT-mTOR, and STATs pathways, as evident from its impact on MAPK, AKT, and STAT3 phosphorylation. Therefore, the ability of hematoxylin to inhibit several types of PTKs and block the downstream signaling molecules raises the possibility that hematoxylin in particular and its analogues in general might be useful lead compounds in cancer therapy or at least useful probes for PTK inhibitor research due to its rich and widely available resources of the raw materials.

We further isolated and structurally elucidated a series of homoisoflavonoids, most of which exhibited potent inhibitory activity on PTKs in the present study. Analysis of the inhibitory potency of all the isolated compounds (**1**−**26**) (Table 5) and their structural features has inferred some regular SAR patterns, which are: (1) For the homoisoflavonoid derivatives, compounds **1**, **2**, **3**, **4**, **6**, **7**, **10**, **11**, **25**, and **26**, with a hydroxyl group at C-8 in ring A to form a catechol fragment, display strong inhibitory activities on PTKs (>80%). Furthermore, compounds with an additional hydroxyl group at C-4 (**1** and **2**), showed much stronger activities than compounds with a methoxyl group (**3** and **4**), a proton (**6**), or a carbonyl group (**7** and **13**) at this position. Compounds **2** and **4** with 4*R**-configuration were more active than compounds **1** and **3** with 4*S**-configuration on c-Src, indicating the stereochemistry of C-4 also related to the activity. Whereas compounds **5**, **12**, **13**, **14**, **15**, **16**, **17**, **18**, and **24**, with a proton at C-8, showed almost no activities, except that the compounds containing a catechol fragment in ring B (**12** and **16**) had weak inhibitory effects. Compounds **8** and **9**, with an α-hydroxy-α,α′-unsaturated ketone moiety in ring A and a catechol fragment in ring B, were inactive due to the different three-dimensional structure compared with hematoxylin. In summary, the catechol moiety in ring A and the hematoxylin-like three-dimensional structure of these homoisoflavonoids were the key essentials for the inhibitory activity on PTKs. The substituent and configuration of C-4 had some relationship with the activity. (2) For the chalcone derivatives, compounds **19** and **20**, with a catechol structural moiety in ring B, displayed moderate inhibitory activities, while compounds **21** and **22**, with a 4,4′-dihydroxyl moiety, were inactive. It was reported first that a series of natural homoisoflavonoids, including hematoxylin, showed potent inhibitory activity on several PTKs. This type of compounds was believed as a new class of interesting PTK inhibitors. Further work is in progress to optimize the structure with the aim of increasing the potency.

Molecular docking analysis provided insight into the action of hematoxylin and three active compounds on c-Src tyrosine kinase in this study. The c-Src kinase domain consists of the characteristic bilobed protein kinase architecture.[25] ATP binds to the cleft between the two major domains and is anchored to the enzyme via hydrogen bonds, metal ions, and polar interactions. Our docking analysis illustrated that these compounds bind to the kinase domain of c-Src in a favorable position for interacting with the amino acid residues located at the entrance of the ATP-binding site, and the two hydroxyl of the catechol groups (ring A) seem to be the most important contributor for the interacting activities through H-bonds with the hinge region. In addition, the second catechol fragment is also predicted to yield extensive hydrophobic and van der Waals interactions with other important residues of c-Src kinase domain, including Asp406 located in the DFG motif, which is critical for ATP binding.[26] Therefore, it is encouraging to note that molecular docking results were quite consistent with the SAR analysis mentioned above. Moreover, docking results clearly indicated that the active compounds are likely to be ATP competitive inhibitors. Further characterization of enzyme kinetics in this study showed hematoxylin to be competitive with ATP, which agrees well with the predicted binding mode based on simulation study.

In summary, an ELISA-based c-Src-targeted high-throughput screening platform was successfully established in this study. With this approach, hematoxylin was first disclosed as a potent c-Src inhibitor and a series of hematoxylin analogues were characterized to be potent hits. The confirmation of multitargeted inhibition and further establishment of SAR analysis with concurrent aid of computational simulation helped unravel the identified homoisoflavonoids as a new class of promising PTK inhibitors, representing these candidates merited for further in vivo evaluation. Comprehensive and critical analysis of parallel

information from natural homoisoflavonoid analogues together with synthetic modifications might hold the promise to lead to the development of much more potent PTK inhibitors.

Experimental Section

General. Optical rotations were taken on a Perkin-Elmer 341 polarimeter. IR spectra were recorded on Nicolet Magna FT-IR 750 spectrophotometer using KBr disks. NMR spectra were recorded on Bruker AM-400 and Varian Unity Inovor-600 NMR spectrometers. The chemical shift (δ) values are given in ppm with TMS as internal standard, and coupling constants (J) are in Hz. EIMS and HREIMS spectra were recorded on Finnigan MAT-95 mass spectrometer. ESIMS and HRESIMS spectra were recorded on Micromass LC-MS-MS mass spectrometer. All solvents were of analytical grade (Shanghai Chemical Plant, Shanghai, P.R. China). Silica gel used for flash chromatography and precoated silica gel GF254 plates used for TLC were produced by Qingdao Marine Chemical Industrials. The TLC spots were viewed at 254 nm and visualized by spraying with 5% sulfuric acid in alcohol containing 10 mg/mL Vanillin. Sephadex LH-20 gel (Amersham Biosciences) and MCI gel (CHP20P, 75−150 μm, Mitsubishi Chemical Industries Ltd.) were used for column chromatography. Preparative HPLC was performed on a Varian SD1 instrument with 320 single wave detector. Chromatographic separation was carried out on a C18 column (220 mm × 25 mm, 10 μm, Merck), using a gradient solvent system comprised of H_2O (A) and CH_3CN (B) at a flow rate of 15 mL/min.

Plant Material. The stems of *H. campechianum* were collected in September 2005 from XiShuangBanNa, Yunnan Province, Southeast of China, and identified by Professor Jin-Gui Shen. A voucher (specimen no. 20050905) was deposited at the herbarium of Shanghai Institute of Materia Medica, Chinese Academy of Sciences.

Extraction and Isolation. The powder of dried stems of *H. campechianum* (14.4 Kg) was extracted with 95% EtOH for three times to give 675 g crude extract. The extract was then suspended in 5 L of water and partitioned with petroleum ether, CH_2Cl_2, EtOAc, and *n*-BuOH successively to give fractions PE (48.7 g), CH (31.4 g), EA (114.1 g), and BU (295 g), respectively.

CH fraction (30 g) was subjected to column chromatography (CC) over silica gel eluted with a gradient of Me_2CO in petroleum ether to yield fractions **1**−**12**. Fraction **5** (2.28 g) was chromatographed on MCI gel eluted with MeOH-H_2O (55:45 to 100:0) to give fractions **5a**−**5e**. Fraction **5a** (115 mg) was passed through Sephadex LH-20 eluted with $CHCl_3$-MeOH (1:1) to yield **5** (8 mg). Fraction **5b** (220 mg) was separated by a silica gel column eluted with $CHCl_3$-MeOH (100:1 to 50:1) to yield compounds **17** (16 mg) and **21** (64 mg). Fraction **5d** (319 mg) was subjected to CC over silica gel eluted with Me_2CO-petroleum ether (6:1 to 3:1) to obtain compounds **18** (32 mg) and **23** (21 mg), respectively. Fraction **8** (1.05 g) was chromatographed on a silica gel column eluted with $CHCl_3$-MeOH (100:1 to 40:1) to obtain compound **22** (462 mg). Fraction **11** (1.7 g) was chromatographed on a MCI gel column eluted with MeOH-H_2O (40:60 to 100:0) to yield four fractions **11a**−**11d**. Compound **20** (68 mg) was obtained by a silica gel column eluted with Me_2CO-petroleum ether (3:1 to 1:1) from **11b** (260 mg). Fraction **11c** (352 mg) was separated over a silica gel column eluted with Me_2CO-petroleum ether (3:1 to 1:1) to give two compounds, **16** (35 mg) and **19** (112 mg).

EA fraction (110 g) was subjected to column chromatography (CC) over silica gel eluted with a gradient of MeOH in $CHCl_3$ to yield fractions **1**−**11**. Fraction **3** (2.56 g) was chromatographed on silica gel eluted with $CHCl_3$-MeOH (40:1 to 6:1) to give fractions **3a**−**3c** and a pure compound **15** (27 mg). Fractions **5b** (120 mg) and **5c** (285 mg) were passed through Sephadex LH-20 eluted with MeOH to yield **14** (56 mg) and **12** (58 mg), respectively. Fraction **6** (6.86 g) was subjected to CC over silica gel eluted with $CHCl_3$-MeOH (20:1 to 3:1) to obtain eight fractions **6a**−**6h**. Fraction **6d** (1.05 g) was chromatographed on a silica gel column eluted with $CHCl_3$-MeOH (20:1 to 10:1) to obtain a mixture of two compounds. Compounds **6** (11 mg) and **11** (32 mg) were isolated from the mixture (120 mg) by preparative HPLC eluted with CH_3CN-H_2O (10:90 to 30:70 in 2 h). Fraction **6h** (1.2 g) was chromatographed on a MCI gel column eluted with MeOH-H_2O (20:80 to 50:50) to yield three subfractions **6h1**−**6h3**. Compound **4** (11 mg) was obtained by preparative HPLC eluted with CH_3CN-H_2O (10:90 to 30:70 in 2 h) from **6h1** (31 mg). Fraction **6h2** (152 mg) was separated by preparative HPLC eluted with CH_3CN-H_2O (10:90 to 35:65 in 2 h) to give two compounds **1** (62 mg) and **2** (13 mg). Fraction **7** (4.4 g) was separated over a MCI gel column eluted with MeOH-H_2O (15:85 to 50:50) to give a major compound **26** (2.2 g) and four fractions **7a**−**d**. Fraction **7a** (84 mg) was purified by preparative HPLC eluted with CH_3CN-H_2O (10:90 to 35:65 in 2 h) to obtain **7** (20 mg). Fraction **8** (30.4 g) was separated by a MCI gel column eluted with MeOH-H_2O (10:90 to 50:50) to give 3 fractions **8a**−**8c**. Fraction **8a** (2.87 g) was chromatographed on a silica gel column eluted with $CHCl_3$-MeOH (10:1 to 1:1) to obtain 3 subfractions **8a1**−**8a3**. **8a1** (210 mg) was further separated by preparative HPLC eluted with CH_3CN-H_2O (10:90 to 35:65 in 2 h) to yield **10** (15 mg) and **25** (32 mg). **8a3** (52 mg) was purified with Sephadex LH-20 to obtain **9** (25 mg). The major constitution of **8a2** and **8b** was compound **26** according to TLC check. Fraction **8c** (205 mg) was further separated to yield compounds **3** (23 mg), **8** (15 mg), **13** (21 mg), and **24** (31 mg) by preparative HPLC eluted with CH_3CN-H_2O (10:90 to 30:70 in 2 h).

Haematoxylol (1). Yellow amorphous powder, $[\alpha]_D^{20}$ +15 (*c* 0.16, MeOH); CD (*c* 1.0 × 10^{-3} mg/mL, MeOH) $\Delta\varepsilon$ −0.29 (277.9), 0 (261.5), +3.11 (236.6), 0 (197.5); UV (MeOH) λ_{max} (log ε) 283 (2.82), 203 (4.07) nm. IR ν_{max} (KBr) 3415 (br), 1697, 1624, 1518, 1481, 1365, 1286, 1200, 1055 cm^{-1}. ^1H and ^{13}C NMR data, see Tables 2 and 3. ESIMS *m/z* 343.0 $[M + Na]^+$, 663.0 $[2M + Na]^+$, 318.9 $[M - 1]^-$, 639.1 $[2M - 1]^-$. HRESIMS *m/z* 343.0789 (calcd for $C_{16}H_{16}O_7Na$, 343.0794).

Epihematoxylol (2). Brown amorphous powder, $[\alpha]_D^{20}$ −11 (*c* 0.15, MeOH); CD (*c* 1.0 × 10^{-3} mg/mL, MeOH) $\Delta\varepsilon$ −0.29 (277.9), 0 (261.5), +3.11 (236.6), 0 (197.5). UV (MeOH) λ_{max} (log ε) 282 (2.63), 202 (3.78) nm. IR ν_{max} (KBr) 3410 (br), 1624, 1481, 1383, 1286, 1057 cm^{-1}. ^1H and ^{13}C NMR data, see Tables 2 and 3. ESIMS *m/z* 343.0 $[M + Na]^+$, 319.0 $[M - 1]^-$, 639.2 $[2M - 1]^-$. HRESIMS *m/z* 343.0782 (calcd for $C_{16}H_{16}O_7Na$, 343.0794).

4-*O*-Methylhematoxylol (3). Brown amorphous powder, $[\alpha]_D^{20}$ +86 (*c* 0.20, MeOH); CD (*c* 1.0 × 10^{-3} mg/mL, MeOH) $\Delta\varepsilon$ −0.29 (277.9), 0 (261.5), +3.11 (236.6), 0 (197.5). UV (MeOH) λ_{max} (log ε) 283 (3.06), 202 (3.57) nm. IR ν_{max} (KBr) 3394 (br), 1701, 1624, 1518 1481, 1363, 1286, 1200, 1055 cm^{-1}. ^1H and ^{13}C NMR data, see Tables 2 and 3. ESIMS *m/z* 356.9 $[M + Na]^+$, 669.0 $[2M + 1]^+$, 667.3 $[2M - 1]^-$. HRESIMS *m/z* 357.0945 (calcd for $C_{17}H_{18}O_7Na$, 357.0950).

4-*O*-Methylepihematoxylol (4). Brown amorphous powder, $[\alpha]_D^{20}$ −9 (*c* 0.20, MeOH); CD (*c* 1.0 × 10^{-3} mg/mL, MeOH) $\Delta\varepsilon$ −0.29 (277.9), 0 (261.5), +3.11 (236.6), 0 (197.5). UV (MeOH) λ_{max} (log ε) 283 (3.04), 203 (3.42) nm. IR ν_{max} (KBr) 3415 (br), 1699, 1618, 1500, 1466, 1259, 1200, 1040 cm^{-1}. ^1H and ^{13}C NMR data, see Tables 2 and 3. ESIMS *m/z* 357.0 $[M + Na]^+$, 691.1 $[2M + Na]^+$, 333.0 $[M - 1]^-$, 667.4 $[2M - 1]^-$. HRESIMS *m/z* 357.0918 (calcd for $C_{17}H_{18}O_7Na$, 357.0950).

Sappanene (5). Yellow amorphous powder. UV (MeOH) λ_{max} (log ε) 284 (3.37), 258 (3.26) nm. IR ν_{max} (KBr) 3423 (br), 1618, 1512, 1450, 1236, 1159 cm^{-1}. ^1H and ^{13}C NMR data, see Tables 2 and 3. EIMS *m/z* 254 M^+ (65), 178 (29), 160 (23), 147 (100), 123 (16), 107 (20). HREIMS *m/z* 254.0940 (calcd for $C_{16}H_{14}O_3$, 254.0943).

Haematoxylene (6). Brown amorphous powder. UV (MeOH) λ_{max} (log ε) 286 (3.49) nm. IR ν_{max} (KBr) 3424 (br), 1623, 1510, 1450, 1238, 1160 cm^{-1}. ^1H and ^{13}C NMR data, see Tables 2 and 4. ESIMS *m/z* 287.0 $[M + 1]^+$, 309.0 $[M + Na]^+$, 595.0 $[2M + Na]^+$, 285.0 $[M - 1]^-$, 571.2 $[2M - 1]^-$. HRESIMS *m/z* 309.0767 (calcd for $C_{16}H_{14}O_5Na$, 309.0739).

Haematoxylone (7). Yellow amorphous powder, $[\alpha]_D^{20}$ +21 (*c* 0.10, MeOH); CD (*c* 1.0 × 10^{-3} mg/mL, MeOH) $\Delta\varepsilon$ −0.29 (277.9), 0 (261.5), +3.11 (236.6), 0 (197.5). UV (MeOH) λ_{max} (log

ε) 291 (3.49), 202 (4.17) nm. IR ν_{max} (KBr) 3325 (br), 1637, 1404, 1095 cm^{-1}. ^1H and ^{13}C NMR data, see Tables 2 and 4. ESIMS *m/z* 357.0 $[M + K]^+$, 316.9 $[M - 1]^-$, 634.9 $[2M - 1]^-$. HRESIMS *m/z* 341.0655 (calcd for $C_{16}H_{14}O_7Na$, 341.0637).

Haematoxin (8). Brown amorphous powder, $[\alpha]_D^{20}$ +206 (*c* 0.20, MeOH); UV (MeOH) λ_{max} (log ε) 323 (7.18), 289 (10.9), 205 (72.7) nm. IR ν_{max} (KBr) 3385 (br), 1641, 1593, 1524, 1383, 1273, 1202, 1097, 1045, 833 cm^{-1}. ^1H and ^{13}C NMR data, see Tables 2 and 4. ESIMS *m/z* 354.9 $[M + Na]^+$, 687.0 $[2M + Na]^+$, 331.0 $[M - 1]^-$, 663.1 $[2M - 1]^-$. HRESIMS *m/z* 355.0797 (calcd for $C_{17}H_{16}O_7Na$, 355.0794).

Epihematoxin (9). Brown amorphous powder, $[\alpha]_D^{20}$ +246 (*c* 0.20, MeOH); UV (MeOH) λ_{max} (log ε) 287 (12.4), 206 (80.9) nm. IR ν_{max} (KBr) 3404 (br), 1643, 1595, 1524, 1383, 1273, 1198, 1109, 1047, 833 cm^{-1}. ^1H and ^{13}C NMR data, see Tables 2 and 4. ESIMS *m/z* 354.9 $[M + Na]^+$, 687.0 $[2M + Na]^+$, 331.0 $[M - 1]^-$, 663.0 $[2M - 1]^-$. HRESIMS *m/z* 355.0800 (calcd for $C_{17}H_{16}O_7Na$, 355.0794).

Isohematoxylin (10). Yellow amorphous powder, $[\alpha]_D^{20}$ −5 (*c* 0.10, MeOH); UV (MeOH) λ_{max} (log ε) 283 (4.3), 201 (42.3) nm. IR ν_{max} (KBr) 3406 (br), 1618, 1508, 1475, 1279, 1059 cm^{-1}. ^1H and ^{13}C NMR data, see Tables 2 and 4. ESIMS *m/z* 325.0 $[M + Na]^+$, 300.9 $[M - 1]^-$, 602.9 $[2M - 1]^-$. HRESIMS *m/z* 325.0673 (calcd for $C_{16}H_{14}O_6Na$, 325.0688).

Materials. The kinase domain of tyrosine kinase c-Src, epidermal growth factor receptor 1 (EGFR/ErbB-1), epidermal growth factor receptor 2 (EGFR-2/ErbB-2), vascular endothelial growth factor receptor 2 (VEGFR-2/KDR), stem cell factor receptor c-kit, and fibroblast growth factor receptor-1 and -2 (FGFR-1, FGFR-2) were expressed using the Bac-to-Bac baculovirus expression system (Invitrogen, Carlsbad, CA) and purified on Ni-NTA columns (QIAGEN Inc., Valencia, CA) as previously described.[27] Vascular endothelial growth factor receptor 1 (VEGFR-1/Flt-1) and platelet derived growth factor receptor β (PDGFRβ) were purchased from Upstate Biotechnology Inc. (Charlottesville, VA). Poly (Glu-Tyr) (4:1), the substrate of tyrosine kinase, was from Sigma, St. Louis, MO. Monoclonal antiphosphotyrosine (PY) antibody PY 99 was purchased from Santa Cruz Biotechnology, Inc.

Compounds Library. Totally, 32200 single compounds were screened in this study. Most of them (32000 compounds) were from the Compound library of National Center for Drug Screening in Shanghai. The others were offered by the chemical research groups of our institute.

Tyrosine Kinase Assays. ELISA HTS assay was conducted with the help of the Beckman Coulter (Fullerton, CA) Biomek FX robotic instrument or automated microtiter plate washer for most manipulations. For most of the compounds from the library, a 10 × 10 orthogonal compound-mixing strategy was used in the primary screening. The tyrosine kinase activities of the purified c-Src kinase domains were determined in 96-well ELISA plates (Corning, NY) precoated with 20 μg/mL Poly $(Glu,Tyr)_{4:1}$ (Sigma, St. Louis, MO). In a typical ELISA assay, 1 μL of 1 mg/mL test compounds or reference standard in DMSO was added to plate wells by the Beckman Coulter Biomek FX robotic instrument. The final DMSO concentration did not exceed 1%, and DMSO controls were employed. Then, 80 μL 5 μM ATP solution diluted in kinase reaction buffer (50 mM HEPES pH 7.4, 20 mM $MgCl_2$, 0.1 mM $MnCl_2$, 0.2 mM Na_3VO_4, 1 mM DTT) was added to each well. Subsequently, the kinase reaction was initiated by the addition of purified tyrosine kinase proteins (20 ng) diluted in 10 μL of kinase reaction buffer solution. After incubation for 1 h at 37 °C, the plate was washed three times with phosphate buffered saline (PBS) containing 0.1% Tween 20 (T-PBS). Next, 100 μL of antiphosphotyrosine (PY99) antibody (1:500 dilution) diluted in T-PBS containing 5 mg/mL BSA was added. After 30 min incubation at 37 °C, the plate was washed three times as before. Horseradish peroxidase-conjugated goat antimouse IgG (100 μL) diluted 1:2000 in T-PBS containing 5 mg/mL BSA was added. The plate was reincubated at 37 °C for 30 min and washed as before. Finally, 100 μL of a solution containing 0.03% H_2O_2 and 2 mg/mL *O*-phenylenediamine in 0.1 M citrate buffer, pH 5.5, was added and samples were incubated at room temperature until color emerged. The reaction was terminated by the addition of 50 μL of 2 M H_2SO_4, and the plate was read using a multiwell spectrophotometer (VERSAmax, Molecular Devices, Sunnyvale, CA) at 490 nm. The inhibition rate (%) was calculated using the following equation: $[1 - (A_{490}/A_{490}\ \text{control})] \times 100\%$. IC_{50} values were obtained by Logit method and were determined from the results of at least three independent tests. The results were analyzed by Graphpad Prism 4.0 software.

Cells and Cell Culture. SK-OV-3 human ovarian carcinoma cells and HT-29 human colorectal adenocarcinoma cells were obtained from the American Type Culture Collection (Rockville, MD). HT-29 cells were cultured in Mccoy's 5A culture medium (Gibco BRL, USA) supplemented with 10% fetal bovine serum (FBS). SK-OV-3 cells were maintained in high-glucose DMEM (GibcoBRL) supplemented with 10% FBS, 100 kIU/L benzylpenicillin, and 100 mg/L streptomycin. All cells were cultured in a humidified atmosphere of 95% air plus 5% CO_2 at 37 °C.

Western Blot Analysis. Cells were grown to half-confluence in six-well plates, starved in serum-free medium for 24 h, and then exposed to hematoxylin at concentration of 2, 10, and 20 μM for 2 h. For analysis of receptor tyrosine kinase phosphorylation and downstream signal transduction pathways, cells were stimulated with 20 ng/mL EGF (from R&D Systems, Minneapolis, MN) for 15 min at 37 °C after hematoxylin treatment. Western blot analyses were subsequently performed as previously described by Guo et al.[28] Antibodies against the following were used: phospho-c-Src and c-Src, phosphopaxillin and paxillin, phospho-ErbB2 and ErbB2, phospho-ERK1/2 and ERK1/2, phospho-AKT and AKT, phospho-PLCγ and PLCγ, phospho-STAT3 and STAT3 (All from Cell Signaling Technology, Beverly, MA) and Actin (Santa Cruz Biotechnology, Santa Cruz, CA).

Molecular Docking Simulation. The high resolution crystal structure of c-Src kinase domain in complex with purvalanol A (PDB entry 1YOM)[29] derived from Protein Data Bank[30] was used as a target for molecular docking simulation. The three-dimensional (3D) structure of hematoxylin was constructed by the Corina program. To further verify the binding model between inhibitors and c-Src protein, molecular docking simulation was performed with Autodock3.05 software.[31] Ligand and water molecules in the crystal structure were removed, polar hydrogens were added, and "KOLLUA" charges[32] were assigned to the protein, and Gasteiger−-Marsilli charges were assigned to the compounds. To ensure the searching space enclosing the binding site, the numbers of grid points were set as 80 in *x*, *y*, and *z* directions around the central point of the active site. The Lamarckian genetic algorithm (LGA)[31] was adopted in the molecular docking simulation, and the number of individuals for the population was set as 150, correspondingly, the maximum number of energy evaluations and the maximum number of generations were set as 4500000 and 81000, respectively. Ten independent runs with different seeds were preformed on a SGI origin3800 supercomputer. The ligand was fully optimized inside the binding site during the docking simulations, and the best docking modes were determined by choosing those poses with the lowest energy for each compound.

Acknowledgment. We thank Prof. Jin-Gui Shen for collecting and identifying the plant material and Dr. Fa-Jun Nan for his useful technical suggestions on high-throughput screening. We appreciate the Department of Analytical Chemistry of SIMM for all spectral measurements. This work was financially supported by grants from the Ministry of Science and Technology (2004CB518902 and 2004CB518903), National Natural Science Foundation of China (C03020705, 30770236), Shanghai Commission of Science and Technology (07DZ05906, 07DZ19728). Hua Xie especially appreciates the financial support by Shanghai Postdoctoral grant (05R214157).

Supporting Information Available: Spectroscopic data of haematoxylol (**1**), epihaematoxylol (**2**), 4-*O*-methylhaematoxylol

(**3**), 4-*O*-methylepihaematoxylol (**4**), haematoxylene (**6**), haematoxylone (**7**), isohematoxylin (**10**), sappanone B (**11**), sappanchalcone (**20**), hematoxylol (**25**), and hematoxylin (**26**). Purity checks for the potent protein tyrosine kinase inhibitors **1**−**4**, **6**, **7**, **10**, **11**, **20**, **25**, and **26** by HPLC with two different mobile phases (CH_3CN-H_2O, 2−25% in 9 min/CH_3OH-H_2O, 5−40% in 15 min). This material is available free of charge via the Internet at http://pubs.acs.org.

References

(1) Traxler, P.; Bold, G.; Buchdunger, E.; Caravatti, G.; Furet, P.; Manley, P.; O'Reilly, T.; Wood, J.; Zimmermann, J. Tyrosine kinase inhibitors: from rational design to clinical trials. *Med. Res. Rev.* **2001**, *21*, 499–512.

(2) Baselga, J. Targeting tyrosine kinases in cancer: the second wave. *Science* **2006**, *312*, 1175–1178.

(3) Plested, J. S.; Coull, P. A.; Gidney, M. A. ELISA Methods. *Mol. Med.* **2003**, *71*, 243–261.

(4) Zhang, X. H.; Guo, X. N.; Zhong, L.; Luo, X. M.; Jiang, H. L.; Lin, L. P.; Ding, J. Establishment of the active catalytic domain of human PDGFRβ tyrosine kinase-based ELISA assay for inhibitor screening. *Biochim. Biophys. Acta.* **2007**, *1770*, 1490–1497.

(5) Irby, R. B.; Yeatman, T. J. Role of Src expression and activation in human cancer. *Oncogene* **2000**, *19*, 5636–5642.

(6) Armstrong, W. P. Logwood and brazilwood: trees that spawned two nations. *Pac. Hortic.* **1992**, *53*, 38–43.

(7) Brown, M. T.; Cooper, J. A. Regulation, substrates and functions of Src. *Biochim. Biophys. Acta* **1996**, *1287*, 121–149.

(8) Namikoshi, M.; Nakata, H.; Nuno, M.; Ozawa, T.; Saitoh, T. Homoisoflavonoids and related compounds. III. Phenolic constitution of *Caesalpinia japonica* SIEB et ZUCC. *Chem. Pharm. Bull.* **1987**, *35*, 3568–3575.

(9) Namikoshi, M.; Nakata, H.; Yamada, H.; Nagai, M.; Saitoh, T. Homoisoflavonoids and related compounds. II. Isolation and absolute configurations of 3,4-dihydroxylated homoisoflavonoids and brazilins from *Caesalpinia sappan* L. *Chem. Pharm. Bull.* **1987**, *35*, 2761–2773.

(10) Namikoshi, M.; Nakata, H.; Saitoh, T. Homoisoflavonoids from *Caesalpinia sappan*. *Phytochemistry* **1987**, *26*, 1831–1833.

(11) Purushothaman, K. K.; Kalyani, K.; Subramaniam, K. Structure of bonducellin: a new homoisoflavonoids from *Caesalpinia bonducella*. *India J. Chem. Sect. B: Org. Chem. Incl. Med. Chem.* **1982**, *21*, 383.

(12) Heller, W.; Andermatt, P.; Schaad, W. A.; Tamm, E. Homoisoflavonone IV. Neue inhaltsstoffe der eucomin-reihe von *Eucomis bicolor*. *Helv. Chim. Acta* **1976**, *59*, 2048–2058.

(13) Kobayashi, M.; Noguchi, H.; Sankawa, U. Formation of chalcones and isoflavones by callus culture of *Glycyrrhiza uralensis* with different production patterns. *Chem. Pharm. Bull.* **1985**, *33*, 3811–3816.

(14) Nagai, M.; Nagumo, S.; Lee, S.-M.; Eguchi, I.; Kawai, K.-I. Protosappanin A, a novel biphenyl compound fromx *Sappan Lignum*. *Chem. Pharm. Bull.* **1986**, *34*, 1–6.

(15) Masuda, H.; Ohtani, K.; Mizutani, K.; Ogawa, S.; Kasai, R.; Tanaka, O. Chemical study on *Haematoxylon campachianum*: a sweet principle and new dibenz[*b*,*d*]oxocin derivatives. *Chem. Pharm. Bull.* **1991**, *39*, 1382–1384.

(16) Namikoshi, M.; Saitoh, T. Homoisoflavonoids and related compounds. IV. Absolute configurations of homoisoflavonoids from *Caesalpinia sappan* L. *Chem. Pharm. Bull.* **1987**, *35*, 3597–3602.

(17) Shimokawa, T.; Kinjo, J.-E.; Yamahara, J.; Yamasaki, M.; Nohara, T. Two novel aromatic compounds from *Caesalpinia sappan*. *Chem. Pharm. Bull.* **1985**, *33*, 3545–3547.

(18) Nicholls, K. W.; Bohm, B. A. Flavonoids and affinities of *Coreopsis bigelovii*. *Phytochemistry* **1979**, *18*, 1076.

(19) Sequist, L. V. Second-generation epidermal growth factor receptor tyrosine kinase inhibitors in non-small cell lung cancer. *Oncologist* **2007**, *12*, 325–330.

(20) Fischer, O. M.; Streit, S.; Hart, S.; Ullrich, A. Beyond Herceptin and Gleevec. *Curr. Opin. Chem. Biol.* **2003**, *7*, 490–495.

(21) Scagliotti, G. V. Potential role of multitargeted tyrosine kinase inhibitors in non-small-cell lung cancer. *Ann. Oncol.* **2007**, *18* (Suppl 10), 32–41.

(22) Stein, M. N.; Flaherty, K. T. CCR drug updates: sorafenib and sunitinib in renal cell carcinoma. *Clin. Cancer Res.* **2007**, *13*, 3765–3770.

(23) Atkins, M.; Jones, C. A.; Kirkpatrick, P. Sunitinib maleate. *Nat. Rev. Drug Discovery* **2006**, *5*, 279–280.

(24) Titford, M. The long history of hematoxylin. *Biotech. Histochem.* **2005**, *80*, 73–78.

(25) Breitenlechner, C. B.; Kairies, N. A.; Honold, K.; Scheiblich, S.; Koll, H.; Greiter, E.; Koch, S.; Schäfer, W.; Huber, R.; Engh, R. A. Crystal structures of active Src kinase domain complexes. *J. Mol. Biol.* **2005**, *353*, 222–231.

(26) Roskoski, R., Jr. Src protein−tyrosine kinase structure and regulation. *Biochem. Biophys. Res. Commun.* **2004**, *324*, 1155–1164.

(27) Zhong, L.; Guo, X. N.; Zhang, X. H.; Wu, Z. X.; Luo, X. M.; Jiang, H. L.; Ding, J. Expression and purification of the catalytic domain of human vascular endothelial growth factor receptor 2 for inhibitor screening. *Biochim. Biophys. Acta* **2005**, *1722*, 254–261.

(28) Guo, X. N.; Zhong, L.; Tan, J. Z.; Li, J.; Luo, X. M.; Jiang, H. L.; Ding, J. In vitro pharmacological characterization of TKI-28, a broad-spectrum tyrosine kinase inhibitor with antitumor and anti-angiogenic effects. *Cancer Biol. Ther.* **2005**, *4*, 1125–1132.

(29) Breitenlechner, C. B.; Kairies, N. A.; Honold, K.; Scheiblich, S.; Koll, H.; Greiter, E.; Koch, S.; Schäfer, W.; Huber, R.; Engh, R. A. Crystal structures of active SRC kinase domain complexes. *J. Mol. Biol.* **2005**, *353*, 222–231.

(30) Berman, H. M.; Westbrook, J.; Feng, Z.; Gilliland, G.; Bhat, T. N.; Weissig, H.; Shindyalov, I. N.; Bourne, P. E. The Protein Data Bank. *Nucleic Acids Res.* **2000**, *28*, 235–242.

(31) Morris, G. M.; Goodsell, D. S.; Halliday, R. S.; Huey, R.; Hart, W. E.; Belew, R. K.; Olson, A. J. Automated docking using a Lamarckian genetic algorithm and an empirical binding free energy function. *J. Comput. Chem.* **1998**, *19*, 1639–1662.

(32) Cornell, W. D.; Cieplak, P.; Bayly, C. I.; Gould, I. R.; Merz, K. M.; Ferguson, D. M.; Spellmeyer, D. C.; Fox, T.; Caldwell, J. W.; Kollman, P. A. A Second Generation Force-Field for the Simulation of Proteins, Nucleic Acids, and Organic Molecules. *J. Am. Chem. Soc.* **1995**, *117*, 5179–5197.

JM701501X